Dynamic Maintenance and Visualization of Molecular Surfaces ⋆

Chandrajit L. Bajaj Valerio Pascucci Ariel Shamir

Department of Computer Sciences and TICAM
University of Texas, Austin, TX 78712

Robert J. Holt Arun N. Netravali

Bell Laboratories, Lucent Technologies, Murray Hill, NJ 07974

Abstract

Molecular surface computations are often necessary in order to perform synthetic drug design. A critical step in this process is the computation and update of an exact *boundary representation* for the molecular surface (e.g. the Lee-Richards surface). In this paper we introduce efficient techniques for computing a molecular surface boundary representation as a set of NURBS (non-uniform rational B-splines) patches. This representation introduces for molecules the same geometric data structure used in the solid modeling community and enables immediate access to a wide range of modeling operations and techniques. Furthermore, this allows the use of any general solid modeling or visualization system as a molecular modeling interface. However, using such a representation in a molecular modeling environment raises several efficiency and update constraints, especially in a dynamic setting. For example, changes in the probe radius result in both geometric and topological changes to the set of patches. Our techniques provide the option of trading accuracy of the representation for the efficiency of the computation, while still tracking the changes in the set of patches. In particular, we discuss two main classes of dynamic updates: one that keeps the topology of the molecular configuration fixed, and a more complicated case where the topology may be updated continuously. In general the generated output surface is represented in a format that can be loaded into standard solid modeling systems. It can also be directly triangulated or rendered, possibly at different levels of resolution, by a standard graphics library such as OpenGL without any additional effort.

⋆ Research supported in part by grants from NSF-CCR 9732306, DMS-9873326, ACI-9982297 and NASA-NCC2-5276

1 Introduction

The high combinatorial complexity of macromolecules makes it challenging to compute and update their structures and properties in real time. Several different approaches have been developed to achieve this efficiency for molecular surface computations [13, 14, 41–43, 45, 46]. Other work on surface representations features the use of metaballs, molecular surfaces, and blobby models [1, 9, 17, 28, 29, 31, 36–38, 48–51]. In this paper we extend this work by describing algorithms that dynamically update and render exact smooth trimmed NURBS (non-uniform rational B-splines) representations for growing the molecular surfaces. Trimmed NURBS are an industry-wide CAD/CAGD standard and fast becoming optimized for graphics rendering software (OpenGL)/hardware [34, 44].

In [5] we present an exact trimmed NURBS boundary representation of the Lee-Richards solvent contact molecular surface [15]. We show in this paper how this trimmed NURBS representation can be efficiently maintained to animate both the solvent accessible surface and the Lee-Richards solvent contact surface of a molecule.

In our approach we combine the use of efficient data structures [20] that have already been shown useful for molecular modeling [26] with the use of standard graphics libraries such as OpenGL and OpenInventor [47]. The basic idea is to dynamically maintain the primary structures and exactly compute and update representations (tensor product rational B-splines, trimmed NURBS) of the molecular surface which are directly displayed by optimized trimmed NURBS rendering functions of OpenGL. In particular we focus on the special case of dynamic, continuous modification of the solvent radius. This allows us to model molecular surfaces with probes of any radius.

We analyze the complexity of two main classes of updates that yield a family of all the molecular surfaces obtained for different solvent radii: (1) updates that keep the Power Diagram [3] fixed (quadratic growing of the radius of the solvent ball); (2) updates that modify the Power Diagram (linear growing of the radius of the solvent ball).

In both cases efficiency is achieved through the introduction of a novel geometric construction. In case (1) we use a new constructive approach to duality that generalizes the standard "lifting" scheme [20], showing that the Power Diagram of a molecule (3D union of balls) constitutes a compact representation of the collection of all the Power Diagrams of the trimming circles of all the patches in a molecular surface. In particular the convex cell of the 3D Power Diagram relative to the ball B is the dual of the 2D Power Diagram of the trimming circles of B. As a first approximation (with the bonus of being

simpler and more efficient) we consider the molecular surfaces obtained by disproportionally increasing the solvent radius so that the associated Power Diagram remains unchanged. We show how we can keep track of the topological changes that occur in the trimming curves of the patches that form the molecular surface so that its boundary representation can be updated efficiently. Furthermore, we compute and dynamically update an exact boundary representation of the molecular surface so that the same dynamic data structure is also suitable for molecular modeling operations such as those supporting synthetic drug design [33].

In previous work on dynamic triangulations the focus has been mostly on the simpler Delaunay/Voronoi structures (unweighted case) [2, 4, 12, 27, 30, 32, 39, 40]. Little has been done on the more general case of dynamic Regular Triangulation/Power Diagrams and for dimensions greater than two. Moreover, the kinds of dynamic operations developed are usually just the insertion/deletion of a single point. Such local operations become inefficient when we need to perform even a simple but global modification. Here we adopt an approach for global modifications where after preprocessing, each patch in the molecular surface is treated independently. By the "dividi et impera" paradigm we increase efficiency by solving several small problems in place of a single large one.

In the case (2) setting, where the 3D Power Diagram is subject to flips, we use the same construction as in [26] based on the definition of a 4D complex of convex polytopes $\mathcal{C}$ whose "horizontal" slices are all the possible 3D Power Diagrams of the growing balls for any growth factor r. Hence we apply a simple hyperplane sweep algorithm to optimally maintain the dynamic Power Diagram of the linearly growing balls. Thus in this case we compute exactly the offset of the union of balls (so that its topology can be precisely determined), even when it requires a change in the nearest neighbor (under power distance) relations among the atoms corresponding to flips in the associated Regular Triangulation. More generally, for a set of balls in d-dimensional space this requires the construction of a complex of convex polytopes in $(d+1)$-dimensional space whose "horizontal" slices are all the possible Power Diagrams.

In either case we prove and also demonstrate (Section 3) that for small solvent radius changes the global topological structure of the molecular surface remains unaltered, requiring only scaling and a dynamic maintenance of the arrangement of domain B-spline trimming curves, and that for large solvent radius changes (Section 4), the regions in which the eventual updates of the topological structure is required is also localized. Both of the constructions are defined in general for unions of growing balls in any fixed dimension.

Our techniques are shown to be general enough to also deal with new smooth molecular surfaces [19] proposed to avoid the singularities that may arise in

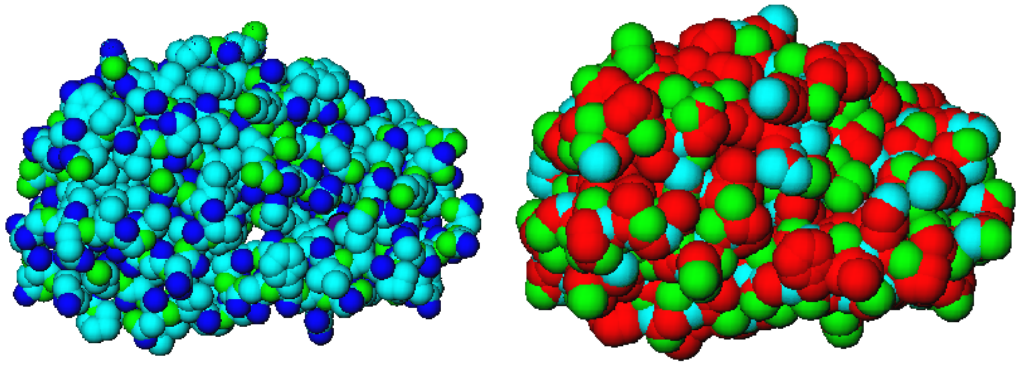

(a) (b)

Fig. 1. The *HIV-2 PROTEASE* (a) and one solvent accessible surface (b) for the same molecule.

the Lee-Richards rolling ball surface. In particular, these procedures can be used to deal with the molecular skin [8, 21], which is a smooth surface comprised of spherical and hyperboloidal patches. As such the molecular skin is similar to the solvent accessible surface with hyperboloidal patches instead of toroidal ones connecting the spherical patches, and in fact uses the same Regular Triangulation/Power Diagram structure, so we can use the same update procedures effectively.

2 Trimmed NURBS Molecular Surface Representation

One of our goals in developing algorithms for automatically maintaining dynamic molecular surfaces is to provide means for immediate display with a standard graphics library like OpenGL without making the additional effort of triangulating the surface as in [1]. To this end we have developed [5] a boundary representation scheme where patches are standard trimmed NURBS. We show in this paper how this data structure can be efficiently maintained to animate the solvent accessible surface (see Figure 1) and the solvent contact surface (see Figure 12) of a molecule. In particular we focus on the special case of dynamic, continuous modification of the solvent radius [1] .

2.1 Regular Triangulation and Power Diagram

Our representation is based upon an underlying structure of the Regular Triangulation of the atom centers in order to define the set of boundary surface patches. The Regular Triangulation and Power Diagram are generalizations of

[1] See the animation in `http://www.ticam.utexas.edu/ccv/projects/VisualEyes/visualization/geomod/surface.html`

the Delaunay Triangulation and Voronoi Diagram, with Euclidean distances replaced by weighted distances. The weight of an atom B with radius r is defined to be $w_B = r^2$. The *power distance* of a general point x in space to B is then defined as

$$\pi_B(x) = \|p - x\|^2 - w_B \quad ,$$

where p is the center of B and $\|p - x\|$ is the ordinary Euclidean distance between p and x. The weighted Voronoi cell of a ball B in a molecule $\mathcal{B}$ is the set of points in space whose weighted distance to B is less than or equal to their weighted distance to any other ball in $\mathcal{B}$ [3, 22]:

$$V_B = \{x \in \Re^3 | \pi_B(x) \leq \pi_C(x) \; \forall C \in \mathcal{B}\} \quad .$$

The Power Diagram of a molecule is the union of the weighted Voronoi cells for each of its atoms. The *weighted Delaunay triangulation*, or *Regular Triangulation*, is the dual of the Power Diagram, where vertices are connected if and only if their corresponding weighted Voronoi cells have a face in common.

2.2 Balls in $\Re^3$ and Halfspaces in $\Re^4$

In this section we introduce the fundamental equations that form the basis of the presented approach for molecular modeling. For a more extensive discussion of the conditions under which the present approach can be extended to a more general case unifying geometries other than spheres, the interested reader is referred to [7]. While for our purposes we deal with $d = 3$, the results are easily extended to arbitrary dimension.

Consider in $\Re^4$ the implicit equation of the unit ball:

$$B_0^4 : \xi_1^2 + \xi_2^2 + \xi_3^2 + \xi_4^2 - 1 \leq 0 \quad . \tag{1}$$

Its boundary has parametric equations which are:

$$\xi_i = \frac{2x_i}{x_1^2 + x_2^2 + x_3^2 + 1} \; , \quad i = 1, 2, 3 \qquad \xi_4 = \frac{x_1^2 + x_2^2 + x_3^2 - 1}{x_1^2 + x_2^2 + x_3^2 + 1} \quad . \tag{2}$$

The boundary of B_0^4 is the closure of the image of $\Re^3$ in $\Re^4$ under the mapping (2). The inverse map of (2) is given by

$$x_i = \frac{\xi_i}{1 - \xi_4} \; , \quad i = 1, 2, 3 \tag{3}$$

for $(\xi_1, \xi_2, \xi_3, \xi_4)$ on the unit sphere $\xi_1^2 + \xi_2^2 + \xi_3^2 + \xi_4^2 = 1$. The point $(0, 0, 0, 1)$ in $\Re^4$ is the image of the point at infinity of $\Re^3$.

Now consider the linear halfspace:

$$h: \quad a_0 + a_1\xi_1 + a_2\xi_2 + a_3\xi_3 + a_4\xi_4 \leq 0 \ , \tag{4}$$

where not all of $\{a_1, a_2, a_3, a_4\}$ are zero. Its pre-image in $\Re^3$, given by the mapping (2), is

$$\begin{aligned} b: \quad & a_0(x_1^2 + x_2^2 + x_3^2 + 1) + a_1\ 2x_1 + a_2\ 2x_2 + a_3\ 2x_3 \\ & + a_4(x_1^2 + x_2^2 + x_3^2 - 1) \leq 0 \ . \end{aligned} \tag{5}$$

If $a_1^2 + a_2^2 + a_3^2 + a_4^2 - a_0^2 \geq 0$ and $a_0 + a_4 > 0$, this is the ball of center $-(a_1, a_2, a_3)/(a_0 + a_4)$ and radius $(a_1^2 + a_2^2 + a_3^2 + a_4^2 - a_0^2)^{1/2}/(a_0 + a_4)$. If $a_1^2 + a_2^2 + a_3^2 + a_4^2 - a_0^2 \geq 0$ and $a_0 + a_4 < 0$, this is the union of the sphere of center $-(a_1, a_2, a_3)/(a_0 + a_4)$ and radius $(a_0^2 - a_1^2 - a_2^2 - a_3^2 - a_4^2)^{1/2}/(-a_0 - a_4)$ and its exterior. When $a_0 + a_4 = 0$, this is a halfspace, and when $a_1^2 + a_2^2 + a_3^2 + a_4^2 - a_0^2 < 0$ and $a_0 + a_4 \neq 0$, this is a ball of imaginary radius, and contains no real points.

A fundamental relationship is that spheres that contain a point (c_1, c_2, c_3) in $\Re^3$ map to hyperplanes that pass through the point $(2c_1, 2c_2, 2c_3, c_1^2 + c_2^2 + c_3^2 - 1)/(c_1^2 + c_2^2 + c_3^2 + 1)$ in $\Re^4$. This is a result of the relation

$$(c_1^2 + c_2^2 + c_3^2 + 1)a_0 + 2(c_1a_1 + c_2a_2 + c_3a_3) + (c_1^2 + c_2^2 + c_3^2 - 1)a_4 = 0 \ .$$

A consequence of this relationship is that a set of spheres passing through two distinct points in $\Re^3$ corresponds to a set of hyperplanes in $\Re^4$ that contain a certain line. Since the actual points of intersection in $\Re^3$ are mapped to points on B_0^4, the unit ball in $\Re^4$, the line in $\Re^4$ must intersect B_0^4 in two points. Spheres in $\Re^3$ that intersect at one point are mapped to hyperplanes whose line of intersection is tangent to B_0^4. Spheres whose combined intersection is empty are mapped to hyperplanes whose line of intersection, if any, does not intersect B_0^4. This situation is illustrated for $d = 2$ in Figure 2. Let l be the line of intersection of the boundaries $\partial h' \cap \partial h''$ corresponding to two distinct intersecting balls b' and b''. We have that $\partial b'$ intersects $\partial b''$ if and only if l intersects B_0^3 (the unit ball in $\Re^3$), that is, if the distance from l to the origin O is smaller than 1:

$$\partial b' \cap \partial b'' = 1 \text{ or } 2 \text{ points} \quad \Longleftrightarrow \quad l \cap B_0^3 \neq \emptyset \quad \Longleftrightarrow \quad \text{dist}(l, O) \leq 1 \ .$$

$$\dim\,(b' \cap b'') = 0 \quad \Longleftrightarrow \quad l \cap B_0^3 = 1 \text{ point} \quad \Longleftrightarrow \quad \text{dist}(l, O) = 1 \ .$$

Similarly we can consider three distinct disks b', b'', and b'''. If their intersection

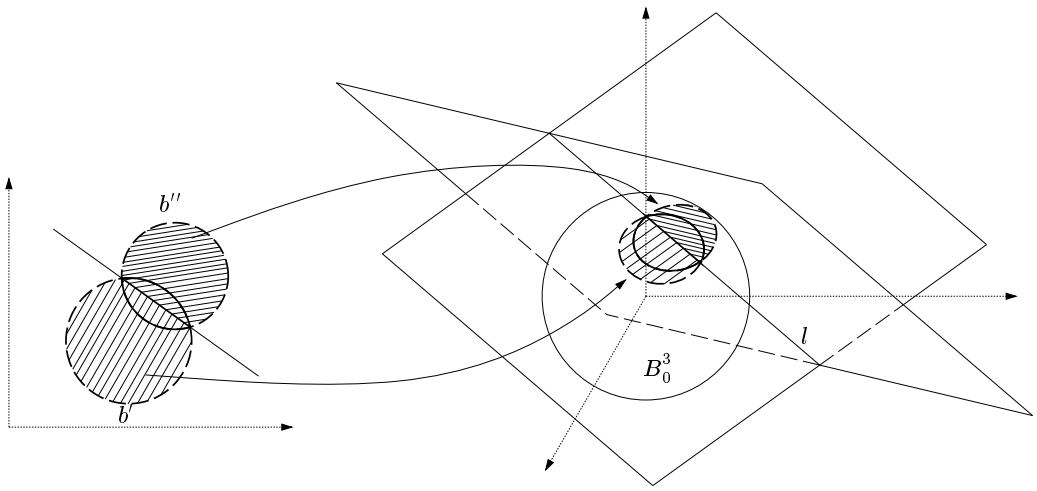

Fig. 2. The intersection between the boundaries of two disks b', b'' in $\Re^2$ corresponds to a line l intersecting the sphere B_0^3.

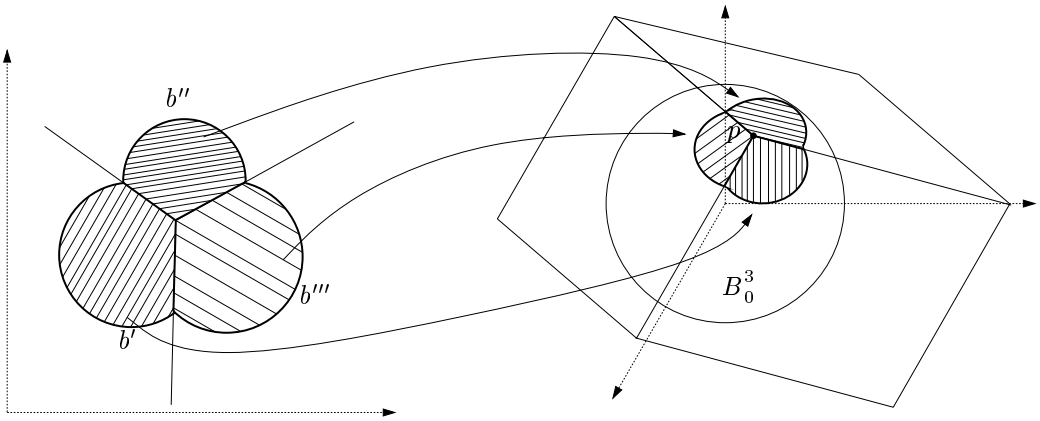

Fig. 3. The non-empty intersection, when bounded by three circular arcs, between three disks b', b'', and b''' in $\Re^2$, corresponds to a point p contained in the ball B_0^3.

is a region bounded by three circular arcs, one from each disk, then the three boundary circles correspond to three planes $\partial h'$, $\partial h''$, and $\partial h'''$ that intersect in a point p contained in B_0^3. This is illustrated in Figure 3. If the three circular boundaries intersect in one or two points, then the planes intersect in a point on ∂B_0^3 (or possibly in a line that intersects B_0^3).

$$b' \cap b'' \cap b''' = \text{ region bounded by 3 arcs (or points)} \iff p \in B_0^3 \quad (6)$$

$$\dim\left(\partial b' \cap \partial b'' \cap \partial b'''\right) = 0 \ . \iff p \in \partial B_0^3 \ .$$

The proof of (6) is given in Appendix A.

Consider the intersection of n balls or their complements, such as $b_1 \cap \bar{b}_2 \cap \bar{b}_3 \cap \cdots \cap b_n$. We can map each of the b_i or $\bar{b}_i$ to a halfspace h in $\Re^{d+1}$ so that the computation of the intersection is reduced to a convex hull computation. Note that if all the balls are complemented we get the complement of the union of balls as in [20]. In general, for the computation of the topological structure of a non-linear, non-convex, possibly disconnected region in $\Re^d$, the intersection of inequalities of the type (5) is reduced to the computation of the boundary of the convex polytope CP, intersection of halfspaces (4), and intersecting this boundary with the unit sphere (1).

This mapping generalizes the "lifting" scheme [18] so that it can represent both the interior and the exterior of balls and so that one can compute any boolean combination of balls instead of just their union. In the present formulation we also represent the balls by their implicit inequality (4) instead of just a center and a radius, so that one can deal with infinite radius spheres (note that such cases arise in practice in the computation of trimming curves).

An additional advantage of the present mapping with respect to the "lifting" scheme is the compact representation of several collections of curve arrangements in the special case of the collection of trimming circles of patches that form a molecular surface. In fact, in this case we need only to observe that the convex polytope CP, that is dual to each arrangement of trimming curves of each patch, is indeed the cell of that patch in the 3-dimensional Power Diagram. This implies we need not represent a separate polytope for each arrangement of trimming curves since the 3-dimensional Power Diagram contains them all. The advantage in storage comes from representing only once any lower-dimensional face shared by more than one polytope. This sharing of faces also provides savings in storage of explicit adjacency information for each boundary curve of each patch.

2.4 Trimmed NURBS Patches

In this section we describe the components of the solvent accessible surface and solvent contact surface are obtained. The solvent accessible surface [14] is the locus of the center of a sphere, or solvent atom, as it rolls along the surface of the molecule. It is equivalent to a union of balls where each the radius of each atom of the original molecule is increased by the radius of the solvent atom. The solvent contact surface [35] is defined as the boundary of the region of space that a solvent atom cannot access because of the presence of the molecule. For the solvent accessible surface (Figure 1), only "convex"

spherical patches are used to create the molecular surface. The solvent contact surface (Figure 12) involves more complex computations including also "saddle" toroidal patches and "concave" spherical patches between the atoms, and the computations of possible self-intersections.

2.4.1 Solvent Accessible Patches

Each atom's spherical patch is the intersection of one sphere (representing the atom) with the exterior of all its neighboring spheres. Let the first sphere be S, and the exterior of a neighboring sphere be R. Then there is a halfspace h such that $S \cap R = S \cap h$. Thus for each atom we can reduce our patch representation problem to the intersection of a sphere with a set of halfspaces.

Given the Voronoi complex of the weighted centers of the molecule atoms, the halfspaces whose common intersection generates the Voronoi cell of the atom B are those with which $S = \partial B$ must be intersected. Since we use a parametric representation $S = f(u, v)$, we need to compute the domain D in (u, v) space such that $f(D) = S \cap h$. Without loss of generality we assume that S is the unit sphere. We adopt the following parametrization:

$$x = \frac{2u}{u^2 + v^2 + 1} \qquad y = \frac{2v}{u^2 + v^2 + 1} \qquad z = \frac{u^2 + v^2 - 1}{u^2 + v^2 + 1} \; . \tag{7}$$

This parametrization maps the (infinite) rectangular domain $[-\infty, +\infty] \times [-\infty, +\infty]$ to the unit sphere. In practice we do not deal with infinite domains since we are only interested in representing proper molecules and not isolated atoms. In order to determine the size of the domain we actually need, assume that we are intersecting S with the halfspace $z \leq d$ (in fact, with translation, rotation, and scaling we always reduce the first intersection to this case). Then in view of (7),

$$z \leq d \Longleftrightarrow \frac{u^2 + v^2 - 1}{u^2 + v^2 + 1} \leq d \Longleftrightarrow u^2 + v^2 \leq \frac{1 + d}{1 - d} \; ,$$

so we can choose the domain D to be the disk centered at the origin with radius $\sqrt{(1 + d)/(1 - d)}$. A change in d corresponds to a scaling of D, that can be performed by simply scaling its control polygon (once a NURBS representation is defined for the trimming curve of D). For any additional cutting halfspace $\bar{h} : Ax + By + Cz \leq D$ originating from other neighboring atoms, we have:

$$(C - D)(u^2 + v^2) + 2(Au + Bv) - (C + D) \leq 0 \; . \tag{8}$$

The trimming curve derived from (8) is the circle

$$\left(u + \frac{A}{C-D}\right)^2 + \left(v + \frac{B}{C-D}\right)^2 = \frac{A^2+B^2+C^2-D^2}{(C-D)^2}$$

unless $C = D$. This occurs only when the plane $Ax+By+Cz = D$ contains the singular point $(0, 0, 1)$ of the parametrization, and in this case the trimming curve is the line

$$Au + Bv - C = 0 \ .$$

The trimming curves are all circles (possibly with infinite radius) so that the domain D can be modeled as the progressive intersection/difference of a sequence of circles.

2.4.2 Solvent Contact Patches

In this section we describe how the convex and concave spherical patches, and saddle toroidal patches of the solvent contact surface S_c are obtained from the molecule and its Power Diagram. Here we will designate the boundary of halfspaces h_i and $\bar{h}_i$ by the planes π_i and $\bar{\pi}_i$.

We first describe the convex spherical patches, and how they relate to the spherical patches of the solvent accessible surface. Let S_a be the solvent accessible surface obtained with a solvent atom of radius r, so that S_a is comprised of spherical patches whose radii are r larger than those of $\mathcal{B}$. In this section we use the Power Diagram and Regular Triangulation of S_a, which are similar to those for $\mathcal{B}$ but with the radii of all atoms increased by r. As shown in Figure 4, let B be an atom of the molecule $\mathcal{B}$ of radius r_0 centered at v, and let the Power Diagram cell of v be the intersection of halfspaces $h_1 \cap \ldots \cap h_k$. Thus B' is the ball of radius $r_0 + r$ centered at v, and B contributes the patch $\partial B \cap h_1 \cap \ldots \cap h_k$ to S_c and $\partial B' \cap \bar{h}_1 \cap \ldots \cap \bar{h}_k$ to S_a. Each boundary hyperplane $\bar{\pi}_i$ is parallel to π_i and is closer to v by the factor $r_0/(r_0 + r)$.

We now consider concave spherical patches. A typical patch is associated with a triangle t of the Regular Triangulation of S_a with vertices v_1, v_2, and v_3, and with a point $\bar{t}$ in the Power Diagram. In this case the solvent atom B_s has no degrees of freedom (it cannot roll since its center is fixed at $\bar{t}$). Define $h(u_1, u_2, u_3; u_4)$ to be the halfspace containing u_1, u_2, u_3 in its planar boundary and u_4 in its interior. Then the contribution of B_s to S_c is given by

$$\partial B_s \cap h(u_1, u_2, \bar{t}; u_3) \cap h(u_3, u_1, \bar{t}; u_2) \cap h(u_2, u_3, \bar{t}; u_1) \ . \tag{9}$$

Saddle toroidal patches are associated with edges in the Regular Triangulation

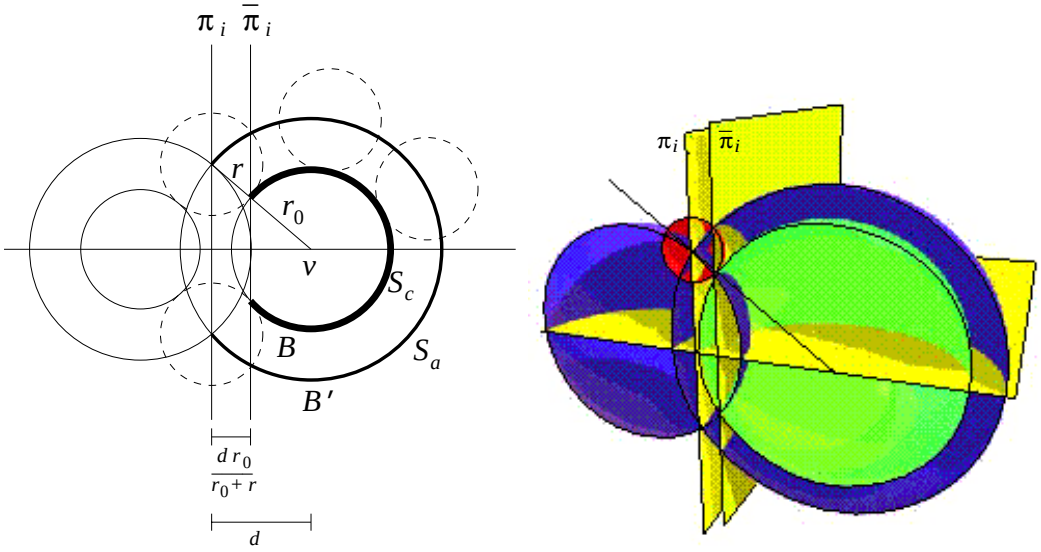

Fig. 4. A solvent atom of radius r rolls on the molecule surface $\mathcal{B}$, maintaining its center on the solvent accessible surface S_a (medium arc). Its point of contact with $\mathcal{B}$ belongs to the solvent contact surface S_c (heavy arc). The plane $\bar{\pi}_i$ marks the border between a convex spherical patch and a saddle toroidal patch.

of S_a. As illustrated in Figure 5, let e be the edge with endpoints v_1 and v_2, the centers of balls B_1 and B_2 with radii r_1 and r_2. Also let B_1' and B_2' be the balls with centers v_1 and v_2 and augmented radii $r_1 + r$ and $r_2 + r$. Then a solid torus E is generated by rolling a probe atom of radius r so that it is constantly tangent to B_1 and B_2, with its center traveling along the circle of intersection $\bar{e}$ of $\partial B_1 \cap \partial B_2$.

Let π be the Voronoi separating plane of B_1 and B_2. As with the convex spherical patches, we can construct two more planes $\bar{\pi}_1$ and $\bar{\pi}_2$ that are parallel to π and closer to v_1 and v_2 by factors $r_1/(r_1+r)$ and $r_2/(r_2+r)$, respectively. The points of contact of the probe sphere with B_1 and B_2 lie on $\bar{\pi}_1$ and $\bar{\pi}_2$, and divide ∂E into two pieces: the inner saddle shaped surface whose cross section is shown with two bold arcs in Figure 5, that is nearer e, and the outer convex surface whose cross section is indicated by dashed arcs. The toroidal patch that is part of the solvent contact surface is the former, and will be denoted by ∂E^*.

If the edge e connects two atoms that do not share another neighbor when the radii of all the atoms are increased by r, then $\bar{e}$ is an entire circle, and all of ∂E^* is part of S_c. Otherwise, the probe atom encounters other atoms, $\bar{e}$ is a sequence of arcs, and the contribution of e to S_c is several toroidal patches bounded by planes parallel to $\overline{v_1 v_2}$. These planes separate toroidal patches from concave spherical patches (see Figure 12), and can simply be taken from the planes that are the boundaries of the halfspaces appearing in (9).

The remaining problem is the removal of (possible) self-intersections that the

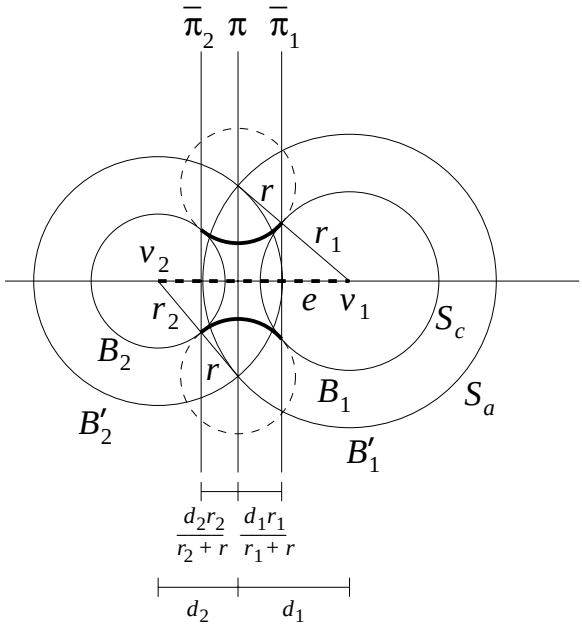

Fig. 5. A solvent atom of radius r rolls on the molecule surface $\mathcal{B}$, maintaining contact with atoms B_1 and B_2 at all times. The inner toroidal patch between the planes $\bar{\pi}_1$ and $\bar{\pi}_2$ is part of the solvent contact surface S_c (heavy arc).

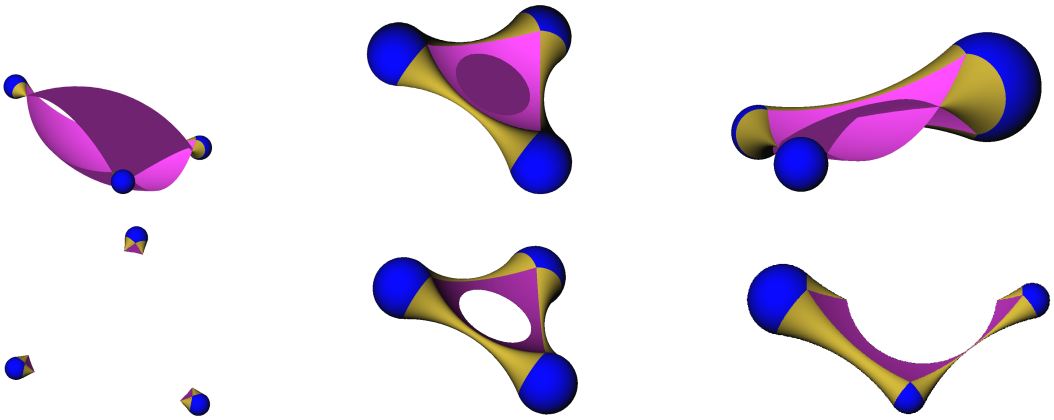

Fig. 6. Three possible self-intersections of the rolling ball surface (top), and the corresponding solvent contact surface (bottom).

rolling ball surface might have (see Figure 6). The solution for this and creation of the actual solvent contact surface is detailed in [5].

3 Maintaining the Molecular Surface Under Quadratic Growth

We call quadratic growth the scheme of growing balls that keeps the Power Diagram unaltered, and thus the topology of the union of balls is given by the corresponding α-shape [23, 24]. Under this growth we only need to maintain

the set of trimming curves of each patch in the surface. In particular we need to efficiently detect any topological changes (new intersections between curves, creation/deletion of connected components) that occur in the trimming curves (circles and lines) in the domain plane.

This goal can be achieved by looking at each patch separately (actually the computation can be performed in parallel for all patches) and classifying the faces of its associated polytope CP with respect to the relative ball B at the current size. This is achieved by using the relations stated in Section 2.2 as follows:

- Each facet of CP that intersects ∂B corresponds to a circle that is effectively involved in the set of trimming curves.
- Each edge of CP that intersects ∂B corresponds to two intersecting circles.

This leads to the following algorithm for maintaining trimming curves. For each face f of CP we determine its minimum distance d_m and its maximum distance d_M from the center of B. This tells us when the circle associated with f is involved in the boundary of the trimming circles. We organize the ranges of all the faces in an interval tree so that we can efficiently perform range queries that are optimal in space and time. While growing the ball B we look at the faces of CP whose range $[d_m, d_M]$ contains the current radius r of B to directly determine the topology of the trimming circles. For example, if the range of a facet of CP contains f but none of its boundary edges, then one of the trimming curves is an entire circle. At the same time this tells us that in the growing process the values of d_m, d_M of the faces of CP constitute the set of "event points" at which the growth of r produces some topological change in the trimming circles. Hence we can efficiently maintain the dynamic arrangement of circles in the plane.

The topological structure of the molecule is given by the Regular Triangulation and its dual, the Power Diagram. We examine the family of triangulations that yield the topological structure of the molecular surfaces (solvent accessible or solvent contact surfaces) while the solvent radius grows. The determination of the topological structure of such molecular surfaces is an important problem addressed by several papers [16]. The family of shapes obtained from a weighted α-shape [20,24] is based on quadratic growth of the radii of the balls and is therefore not directly related to the family based on the growth of the solvent ball radius. In fact the fundamental property on which the α-shape construction is based on is that for any α, the Power Diagram/Regular Triangulation remains the same. This is achieved by growing each sphere by a different amount, namely the radius of each sphere is augmented by a quantity such that the square of each radius is increased by the same quantity (see Figure 7). This implies that smaller spheres are grown more than the larger ones. As a consequence the resulting surface does not reflect exactly the required

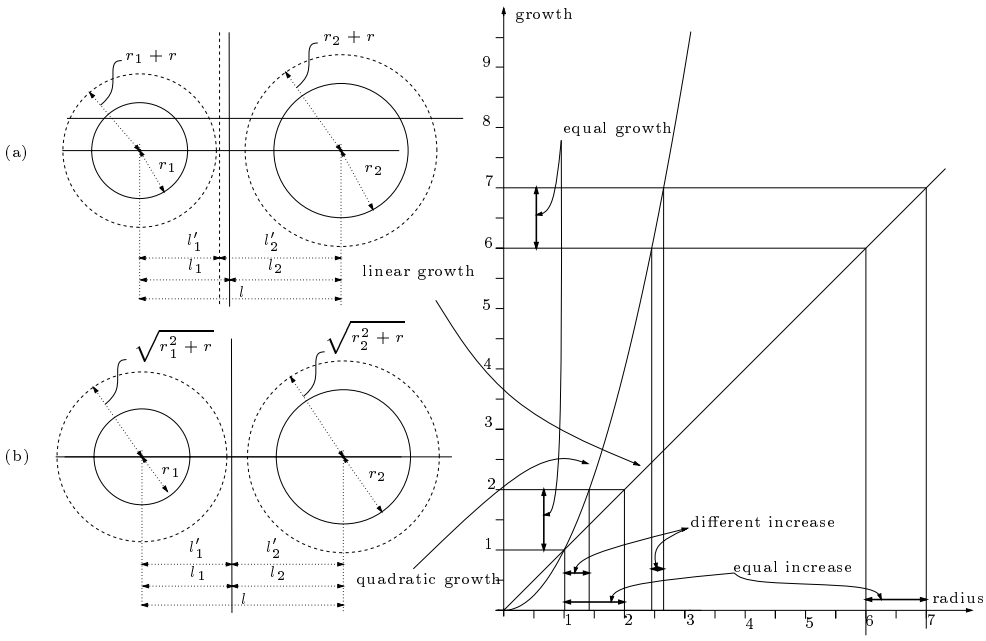

Fig. 7. (a) If the radii of two balls are incremented by the same amount, then their Voronoi separator moves towards the smaller one. (b) If the squares of the radii of two balls are incremented by the same amount, then their Voronoi separator remains the same.

molecular surface (see Figure 8). When this level of approximation (possibly incorrect both in geometry and in topology) is not satisfactory, one needs to resort to the method introduced in the following section.

4 Maintaining the Molecular Surface under Linear Growth

The fundamental dynamic setting we consider is the case of a global linear growth of all the atoms of a molecule, corresponding to a linear growth of the solvent atom radius r. In this case the Voronoi (or more exactly Power Diagram) plane that separates the two balls moves as a function of r, resulting in topological changes of the triangulations and in the set of NURBS patches defining the molecular surface (see Figure 9). In fact, as the radius of each ball is increased by r, the Voronoi plane that separates the two balls moves towards the smaller ball. For example in Figure 7, the distances l_1, l_2 of the Voronoi plane π from the centers of the two balls must be such that the power distances of π are equal, that is:

$$l_1^2 - r_1^2 = l_2^2 - r_2^2 \ .$$

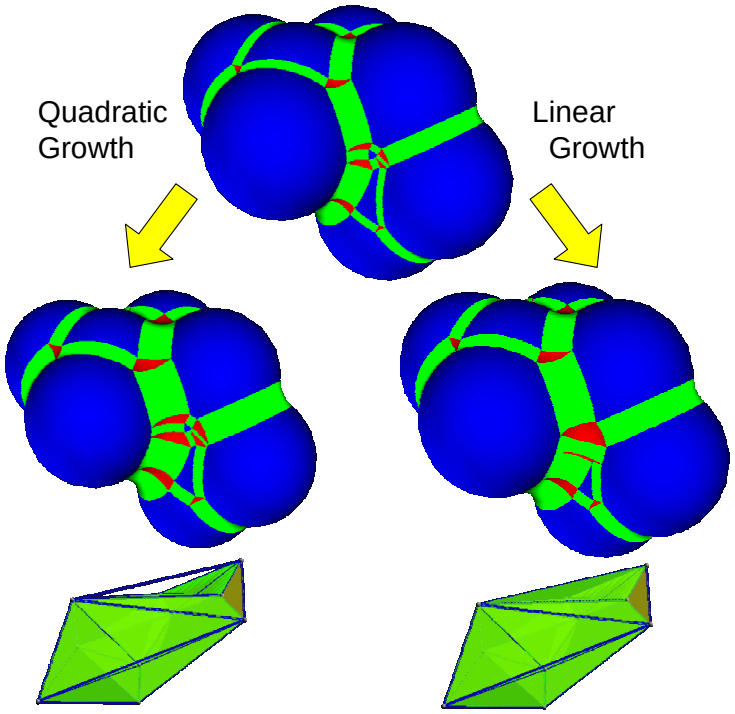

Fig. 8. The difference between a quadratic and a linear growth of the molecule for a given probe radius. The molecular surface (top) is grown quadratically (middle left), hence maintaining the topology of the set of patches, giving an approximation to the real molecular surface computed by linear growth (middle right). The topology differences can be seen in the weighted zero alpha shapes (bottom) from a different viewpoint.

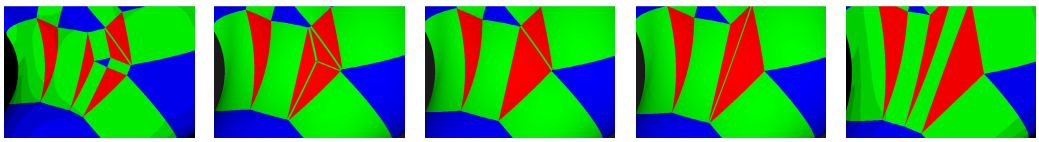

Fig. 9. Examples of several topological changes in the set of NURBS patches, while growing the probe radius linearly.

Moreover, the distance between the two balls is constant (the two balls grow but do not move):

$$l_1 + l_2 = l \ .$$

From these two equations we obtain for l_1:

$$l_1^2 - r_1^2 = (l - l_1)^2 - r_2^2 = l^2 + l_1^2 - 2l_1 l - r_2^2$$

$$l_1 = \frac{l^2 + r_1^2 - r_2^2}{2l} \ .$$

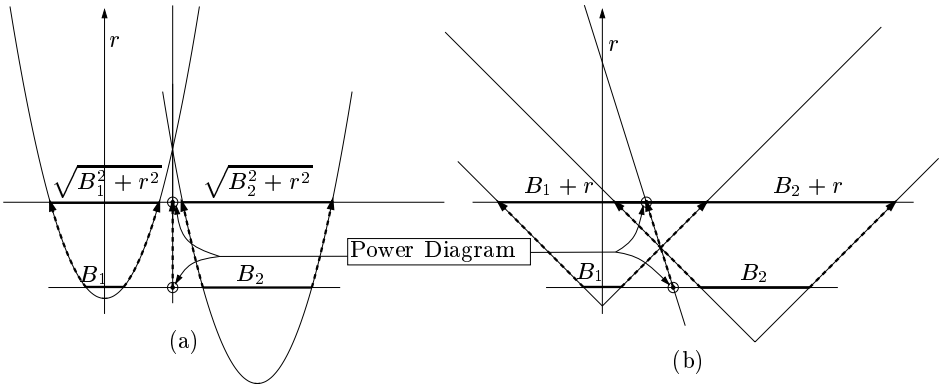

Fig. 10. The 1-dimensional case of ball growth. The quadratic growth (a) keeps the Power Diagram hyperplane (a point) still. The linear growth (b) moves the Power Diagram hyperplane linearly with r.

When r_1 and r_2 change to $r_1 + r$ and $r_2 + r$ we have:

$$l_1 = \frac{l^2 + (r_1 + r)^2 - (r_2 + r)^2}{2l} = \frac{l^2 + r_1^2 - r_2^2 + 2r(r_1 - r_2)}{2l} \ .$$

In general, consider two balls B_1, B_2 (of radii r_1 and r_2 respectively) in $\Re^d$ and assume, without loss of generality, a coordinate system with the center of B_1 at the origin and the center of B_2 on the positive x_1 axis (say at $(l, 0, \ldots, 0)$). The hyperplane of the Power Diagram that separates B_1 from B_2 has the equation:

$$\pi : \qquad x_1 = \frac{l^2 + r_1^2 - r_2^2}{2l} + r\frac{2(r_1 - r_2)}{2l} \tag{10}$$

which is linear in r. Hence this is also a hyperplane in the $(d+1)$-dimensional space $(x_1, \ldots, x_d, r)$. Figure 10 shows the 1-dimensional case of two balls (segments) that grow quadratically (a) or linearly (b). In the first case the hyperplane of the Power Diagram that separates B_1 from B_2 remains the same for all values of r. In the second case, the hyperplane of the Power Diagram that separates B_1 from B_2 moves linearly with r with a slope towards the center of B_1.

This fundamental observation leads to the construction of the Power Diagram of a set of growing balls as the intersection of a hyperplane $r = const$ with a complex $\mathcal{C}$ of convex polytopes in the $(d+1)$-dimensional space $(x_1, \ldots, x_d, r)$. If the molecule $\mathcal{B}$ is composed of n balls $\{B_1, \ldots, B_n\}$ then the complex $\mathcal{C}$ is a collection of n convex polytopes $\{C_1, \ldots, C_n\}$, one per ball. In particular the cell C_i associated with the ball B_i is the intersection of all the halfspaces of points "nearer" to B_i than to B_j (with $j = 1, \ldots, i-1, i+1, \ldots, n$). The boundary hyperplane of such halfspaces is given by equation (10). Note that cell C_i is defined as the intersection of all possible $n+1$ halfspaces since by

linear growing many flips can occur in the Regular Triangulation. A flip occurs when an edge connecting two opposite vertices of a quadrilateral comprising two triangles in the triangulation is replaced by the edge connecting the other two vertices, as illustrated for the 2-dimensional case in Figure 11. The brute force application of the technique as described here requires the computation of n convex hulls [11] in four-dimensional space, which leads to an $O(n^3)$ time worst case complexity. For our purposes this is just a preprocessing step needed to construct the data structure used for animating the molecular surface, so we do not report in the present paper the details of an efficient computation of this complex $\mathcal{C}$. Note however, that in the case of a molecule in three dimensions ($d = 3$) we have to compute a set of 4-dimensional convex hulls that can be computed more efficiently, in an output sensitive sense, by using the algorithm given in [10]. The use of this algorithm would indeed be beneficial because the overall number of faces in $\mathcal{C}$ is indeed $O(n^2)$. This is proved by a technique introduced in [7] that generalizes the "lifting" scheme for the computation of Power Diagrams [18] and maps the construction of the complex $\mathcal{C}$ to a convex hull computation (intersection of halfspaces) in one dimension higher (that is in dimension $d + 2$). In the case of a molecule in three dimensions, this leads to the computation of the convex hull in dimension five that can be computed optimally [11] in $O(n^2)$ time. This is certainly optimal in odd dimension (and in particular in the case of molecules where $d = 3$) since a single Power Diagram (and $\mathcal{C}$ contains many of them) already has the same number of faces as a $(d + 1)$-dimensional convex polytope.

In the previous section we introduced the construction of a complex of convex polytopes $\mathcal{C}$ embedded in the $(d + 1)$-dimensional space $(x_1, \ldots, x_d, r)$ whose "horizontal" slices (that is an intersection with the hyperplane $r = const$) are the Power Diagrams of the balls $\mathcal{B}$ with radii uniformly increased by r. This data structure allows us to animate (update) efficiently the representation of a molecular surface (solvent accessible or solvent contact) with respect to a change in the solvent radius. In particular we can achieve simple and efficient updates on the Power Diagram localized in regions where the topological changes actually occur. In this way we can then in turn directly apply the method described in Section 3.

Being that the Power Diagram is the intersection of a horizontal hyperplane $H : r = const$ with the complex $\mathcal{C}$, in the dynamic setting the linear growth of the radii is simply a sweep of such horizontal hyperplanes H along the r-axis. Hence the "event points" at which we have to update the topological structure of the Power Diagram are the vertices of $\mathcal{C}$. In particular to compute these hyperplane sections of $\mathcal{C}$ we apply the robust approach in [6] which is based on the robust "above or below" classification of the vertices of $\mathcal{C}$ with respect to H. We sort the vertices of $\mathcal{C}$ by their r coordinates so that their classification is obtained in logarithmic time by locating the current height value of H in such a sorted list of vertices. This approach is also suitable for the dynamic growth

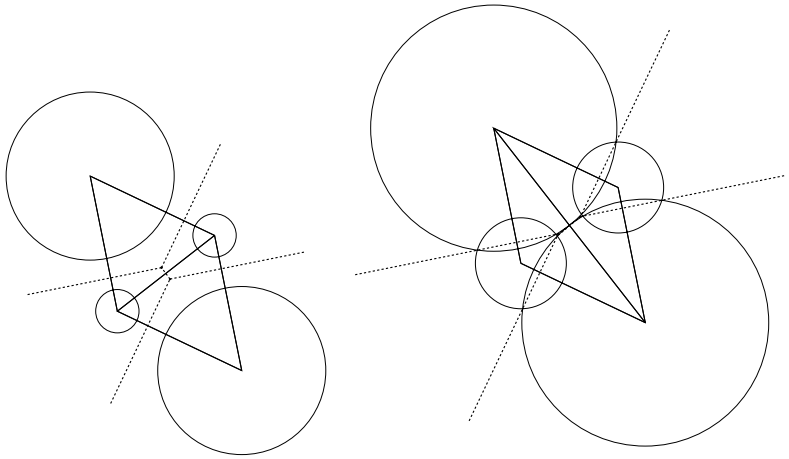

Fig. 11. A simple case of a Regular Triangulation for which the topology changes in a simple linear growth of the radius of the balls.

setting in which we will be continuously moving the hyperplane H. In fact in such a scenario, each time we cross a vertex of $\mathcal{C}$, we will need to update only the cells incident to this vertex. Moreover in general, if we suddenly change our solvent radius from a value r_1 to a value r_2, we will be able to detect the vertices whose r coordinate is in the range $[r_1, r_2]$, change their above/below classification and consequently update all the incident faces of $H \cap \mathcal{C}$. We reach the conclusion that when spheres grow linearly, some flips can occur in the Regular Triangulation, unlike the quadratic growth, so that the usual α-shape construction is invalid (see Figure 11).

5 Implementation Details and Examples

In this section we describe the implementation details of our algorithm. First, a complex corresponding to the molecule is constructed. Second, we sweep a hyperplane across the complex and record the topology changes, or flips [25], that occur, and perform those flips that are between given initial and final probe radii. For each topology, we compute the trimming curves for all of the intersections of atoms. These trimming curves, together with the atom center locations, then allow us to reconstruct the molecular surface patches in 3-space.

The first stage in the implementation is a preprocessing step. We construct the complex $\mathcal{C}$, and then let the hyperplane H sweep along the r-axis from $r = -\infty$ to $r = +\infty$ and record the flips [25] that occur dynamically. Second, once an array of flips sorted by r is obtained, we perform the flips that are between the initial probe radius r_1 and the destination probe radius r_2.

Figure 12 illustrates an example of how the smoothed molecular surface

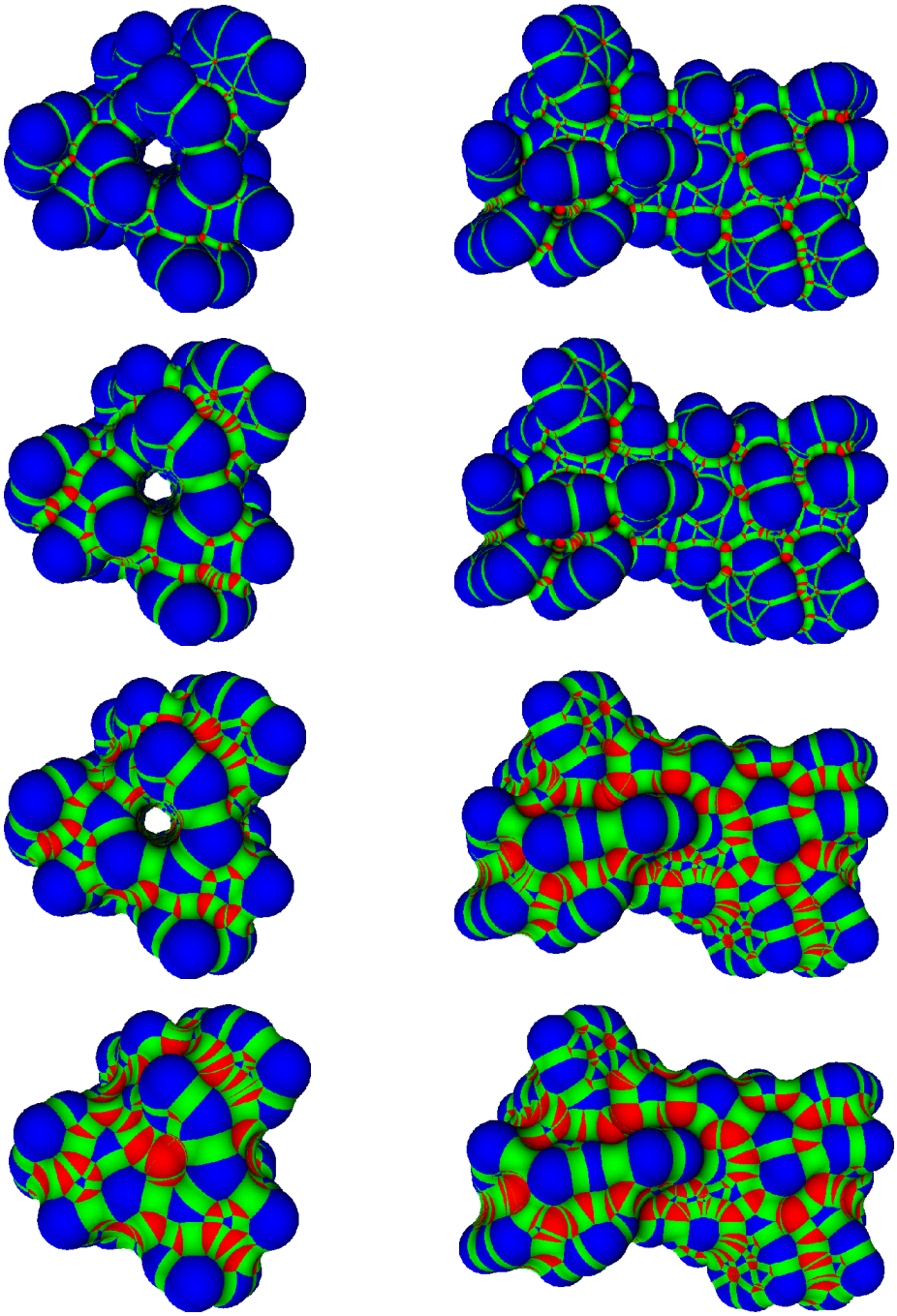

Fig. 12. Several snapshots in two views of a dynamic molecular surface in which the radius of the probe atom is grown linearly. The individual molecule atoms are colored blue. Patches between two and three atoms are colored green and red, respectively. As can be seen, the topology of the union of patches changes over time.

changes as the radii of the atoms grow linearly. As the atoms grow, some of the interior balls are engulfed. Also the patches interpolating three atoms tend to get consistently wider.

In the following two subsections we provide detailed development of the

method for two relatively simple cases. Any general setting can easily be converted to those cases by locally translating to the origin, scaling to a unit sphere, and rotating the related atom. This implies we need only one NURBS spherical patch representation in our implementation, corresponding to this atom position and scale. We then compute the trimming curves from the neighboring atoms with given expressions that are precoded instead of recomputing them every time in the general position. To place the result in the correct position in the molecule we apply the inverse mapping to the control points of the trimmed NURBS patch. This mapping is not applied to the trimming curves themselves since they are defined in the parameter space of the NURBS patch.

The two following examples show the details of the trimming curves computation in the case of Figure 2. In particular Figure 13(a) shows a section of the ball B of Figure 2 along a plane ξ_1-ξ_2 orthogonal to the line l. The other possible case is shown in Figure 3 where the start and end points of the trimming curve result from the intersection of π_1 with different planes. Is this case one can easily compute a new plane π_2 (distinct from π_1) through the two end points and use it to compute the trimming curve parameters in the same way as the previous case.

5.1 Example 1

Here we choose a coordinate system so that two of the balls have centers on the ξ_1-axis in $\Re^3$. Specifically, consider three balls B', B'', and B'''. Choose a coordinate system so that their centers are located at $(0,0,0)$, $(l_{12},0,0)$, and $(l_{13}\cos\beta, l_{13}\sin\beta, 0)$, where l_{12} and l_{13} are the distances between the centers of B' and B'', and between the centers of B' and B''', respectively, and β is the angle made by the three centers, with B' at the vertex. We can assume $0 < \beta < \pi$. Let the solvent ball have radius r.

We consider the two planes π_1, π_2 relative to two trimming curves c_1, c_2. The position of the line $l = \pi_1 \cap \pi_2$ of intersection is used to track the intersection between c_1 and c_2 and to give their 2D NURBS representation.

With the above coordinate system, the two planes have equations (see Figure 13):

$$\pi_1 : \xi_1 = a_1 + r a_2$$
$$\pi_2 : (\cos\beta)\xi_1 + (\sin\beta)\xi_2 = a_3 + r a_4$$

where

$$a_1 = \frac{l_{12}^2 + r_1^2 - r_2^2}{2l_{12}} \qquad a_2 = \frac{r_1 - r_2}{l_{12}} \qquad a_3 = \frac{l_{13}^2 + r_1^2 - r_3^2}{2l_{13}} \qquad a_4 = \frac{r_1 - r_3}{l_{13}} \; .$$

in accordance with (10).

The image of the trimming curve is the intersection of the spherical surfaces of the balls $B'(r)$ and $B''(r)$, which we define as the balls of radii $r_1 + r$ and $r_2 + r$ centered at $(0, 0, 0)$ and $(l_{12}, 0, 0)$, respectively. The implicit equation of the spherical surface of $B'(r)$ is then $\xi_1^2 + \xi_2^2 + \xi_3^2 = (r_1 + r)^2$, and one finds that the ξ_3 coordinate of the two points of intersection between this sphere and the line l is

$$\xi_3 = \pm\sqrt{(r_1 + r)^2 - \xi_1^2 - \xi_2^2}$$

The segment of the line $l = \pi_1 \cap \pi_2$ within $B'(r)$ then has the parametrization:

$$\begin{aligned}
&\xi_1 = a_1 + r a_2 \\
&\xi_2 = a_5 + r a_6 \\
&\xi_3 = \sqrt{(r_1 + r)^2 - (a_1 + r a_2)^2 - (a_5 + r a_6)^2}\; u \quad , \\
&-1 \le u \le 1 \quad ,
\end{aligned}$$

where

$$a_5 = \frac{a_3 - a_1 \cos\beta}{\sin\beta} \quad a_6 = \frac{a_4 - a_2 \cos\beta}{\sin\beta} \quad .$$

For brevity, these quantities which will appear frequently in the sequel will be named as follows. Keep in mind that all of these b_i are functions of r.

$$\begin{aligned}
&b_1 = r_1 + r \qquad b_2 = a_1 + r a_2 \qquad b_3 = a_3 + r a_4 \qquad b_4 = a_5 + r a_6 \\
&b_5 = \sqrt{b_1^2 - b_2^2 - b_4^2} \qquad b_6 = \sqrt{b_1^2 - b_2^2} \qquad b_7 = \sqrt{b_2^2 + b_4^2} \qquad .
\end{aligned}$$

To map the surface of the ball $B'(r)$ to a plane, we use an inverse mapping similar to (3) but for a sphere of radius $r_1 + r$ instead of 1 and specifically $d = 2$:

$$x_1 = \frac{\xi_1}{r_1 + r - \xi_3} \qquad x_2 = \frac{\xi_2}{r_1 + r - \xi_3} \quad .$$

From this one obtains the intersection points q_1 and q_7 (see Figure 13(b); these points lie on a line through the origin) in the $(x_1(r), x_2(r))$ parameter space as

$$q_1 = \left(\frac{b_2}{b_1 + b_5}, \frac{b_4}{b_1 + b_5}\right) \qquad q_7 = \left(\frac{b_2}{b_1 - b_5}, \frac{b_4}{b_1 - b_5}\right) \quad .$$

and the trimming curve is an arc of the circle with center

$$q_0 = \left(\frac{b_1}{b_2}, 0\right)$$

and radius

$$\frac{b_6}{b_2} \ .$$

One next needs to find suitable break points q_3 and q_5 (see Figure 13). Ideally we want none of the arcs $q_1\widehat{q}_3$, $q_3\widehat{q}_5$, $q_5\widehat{q}_7$ to be close to 180°. We can make sure that none of these arcs exceeds 120° as follows. Let q_8 be the midpoint of segment $\overline{q_1q_7}$, and let q_9 be the intersection of the perpendicular bisector of $\overline{q_1q_7}$ with the arc $q_3\widehat{q}_5$. Now choose q_3 and q_5 to be on the line perpendicular to $\overleftrightarrow{q_8q_9}$ that intersects $\overleftrightarrow{q_8q_9}$ at a point 3/4 of the way from q_8 towards q_9. In the limiting case when q_1 and q_7 coincide, which occurs when $(r_1 + r)^2 = (a_1 + ra_2)^2 + (a_5 + ra_6)^2$, the three arcs $q_1\widehat{q}_3$, $q_3\widehat{q}_5$, $q_5\widehat{q}_7$ are all 120°, and they all shrink as the arc $q_1 - q_3 - q_5 - q_7$ shrinks.

In the x_1x_2-plane, line $\overleftrightarrow{q_1q_7}$ has the equation $(a_5 + ra_6)x - (a_1 + ra_2)y = 0$. We also have

$$q_8 = \left(\frac{b_1b_2}{b_7^2}, \frac{b_1b_4}{b_7^2}\right) \ , \qquad q_9 = \left(\frac{b_1}{b_2} + \frac{b_4b_6}{b_2b_7}, -\frac{b_6}{b_7}\right) \ .$$

From this we get

$$q_3 = \left(\frac{4b_1b_7^2 - b_1b_4^2 + 3b_4b_6b_7}{4b_2b_7^2} - \frac{\sqrt{6b_1^2b_4^2 + 7b_2^2b_5^2 + 6b_1b_4b_6b_7}}{4b_7^2}, \right.$$
$$\left. \frac{b_1b_4 - 3b_6b_7}{4b_7^2} - \frac{b_4\sqrt{6b_1^2b_4^2 + 7b_2^2b_5^2 + 6b_1b_4b_6b_7}}{4b_2b_7^2}\right)$$
$$q_5 = \left(\frac{4b_1b_7^2 - b_1b_4^2 + 3b_4b_6b_7}{4b_2b_7^2} + \frac{\sqrt{6b_1^2b_4^2 + 7b_2^2b_5^2 + 6b_1b_4b_6b_7}}{4b_7^2}, \right.$$
$$\left. \frac{b_1b_4 - 3b_6b_7}{4b_7^2} + \frac{b_4\sqrt{6b_1^2b_4^2 + 7b_2^2b_5^2 + 6b_1b_4b_6b_7}}{4b_2b_7^2}\right) \ .$$

We now determine q_2, q_4, and q_6 as the points of intersection of the tangent lines through q_1, q_3, q_5, and q_7. We get

$$q_4 = \left(\frac{-7b_1^2b_4^3 + 4b_1^2b_4b_7^2 - 12b_1b_6b_7^3 - 7b_2^2b_4b_5^2 - 9b_4b_6^2b_7^2}{4b_2b_7^2(b_1b_4 - 3b_6b_7)}\ , \right.$$
$$\left. \frac{7b_1^2b_4^2 + 7b_2^2b + 5^2 + 9b_6^2b_7^2}{4b_2b_7^2(b_1b_4 - 3b_6b_7)} \right) \quad .$$

Also

$$\begin{aligned} q_2 = (1/d_1)\ \Big(b_2[&7b_1^3b_2^2b_4^3 + 7b_1^3b_4^5 - 4b_1^3b_4^3b_7^2 + 7b_1^2b_2^2b_4^3b_5 + 4b_1^2b_2^2b_4b_5b_7^2 \\ &+ 7b_1^2b_4^5b_5 - 4b_1^2b_4^3b_5b_7^2 + 12b_1^2b_4^2b_6b_7^3 + 7b_1b_2^4b_4b_5^2 + 7b_1b_2^2b_4^3b_5^2 \\ &- 4b_1b_2^2b_4^3b_7^2 + 13b_1b_2^2b_4b_6^2b_7^2 - 12b_1b_2^2b_5b_6b_7^3 + 9b_1b_4^3b_6^2b_7^2 + 12b_1b_4^2b_5b_6b_7^3 \\ &+ 7b_2^4b_4b_5^3 + 7b_2^2b_4^3b_5^3 + 12b_2^2b_4^2b_6b_7^3 + 9b_2^2b_4b_5b_6^2b_7^2 - 12b_2^2b_6^3b_7^3 \\ &+ 9b_4^3b_5b_6^2b_7^2 + (-4b_1^2b_2b_4b_7^2 - 8b_1b_2b_4b_5b_7^2 + 4b_2b_4^3b_7^2 - 4b_2b_4b_6^2b_7^2)c_1], \\ &7b_1b_2^2b_4^2b_5^4 + 7b_1b_2^4b_5^2b_6^2 + 7b_1b_2^2b_4^2b_5^2b_6^2 + 7b_1^2b_2^2b_4^2b_5^3 + 7b_2^2b_4^2b_5^3b_6^2 \\ &+ 12b_1^2b_4b_6^3b_7^3 + 9b_1b_4^2b_6^4b_7^2 + 7b_1^2b_2^2b_4^2b_5b_6^2 - 12b_2^2b_4b_6^3b_7^3 + 7b_1^3b_2^2b_4^2b_6^2 \\ &+ 9b_1^2b_2^2b_5b_6^2b_7^2 - 12b_1b_2^2b_4b_5b_6b_7^3 - 4b_1b_2^2b_4^4b_7^2 + 7b_1^4b_2^2b_4^2b_5 - 4b_1^4b_4^2b_5b_7^2 \\ &+ 4b_1^2b_2^2b_4^2b_5b_7^2 + 9b_1b_2^2b_6^4b_7^2 + 7b_1^2b_4^4b_5b_6^2 - 4b_1^3b_4^2b_6^2b_7^2 + 4b_1b_2^2b_4^2b_6^2b_7^2 \\ &- 4b_1^3b_4^2b_5^2b_7^2 + 9b_1b_2^2b_5^2b_6^2b_7^2 + 12b_1^2b_4b_5^2b_6b_7^3 + 9b_1b_4^2b_5^2b_6^2b_7^2 \\ &+ 12b_1^3b_4b_5b_6b_7^3 + 7b_1^3b_2^2b_4^2b_5^2 + 5b_1^2b_4^2b_5b_6^2b_7^2 + 9b_2^2b_5b_6^4b_7^2 \\ &+ 12b_1b_4b_5b_6^3b_7^3 + 9b_4^2b_5b_6^4b_7^2 + 7b_1^3b_4^4b_6^2 + 7b_1^4b_4^4b_5 + 7b_1^3b_4^4b_5^2 \\ &+ 7b_1b_2^4b_5^4 + 7b_2^4b_5^3b_6^2 + 7b_1^2b_2^4b_5^3 + 12b_2^2b_4^3b_6b_7^3 \\ &+ (-4b_1^3b_2b_5b_7^2 - 4b_1^2b_2b_5^2b_7^2 - 4b_1^2b_2b_6^2b_7^2 + 4b_1b_2^3b_5b_7^2 \\ &\quad -4b_1b_2b_5b_6^2b_7^2 - 4b_2^3b_4^2b_7^2 + 4b_2^3b_6^2b_7^2)c_1\Big) \end{aligned}$$

and

$$\begin{aligned} q_6 = \frac{1}{d_2}\ \Big(b_2[&4b_1^2b_4^3b_5b_7^2 - 9b_2^2b_4b_5b_6^2b_7^2 - 12b_1b_4^2b_5b_6b_7^3 - 9b_4^3b_5b_6^2b_7^2 + 7b_1^3b_4^5 \\ &+ 12b_1^2b_4^2b_6b_7^3 + 9b_1b_4^3b_6^2b_7^2 - 7b_1^2b_2^2b_4^3b_5 + 12b_2^2b_4^2b_6b_7^3 - 12b_2^2b_6^3b_7^3 \\ &+ 12b_1b_2^2b_5b_6b_7^3 - 4b_1^2b_2^2b_4b_5b_7^2 + 13b_1b_2^2b_4b_6^2b_7^2 + 7b_1^3b_2^2b_4^3 - 7b_1^2b_4^5b_5 \\ &- 4b_1^3b_4^3b_7^2 - 4b_1b_2^2b_4^3b_7^2 - 7b_2^4b_4b_5^3 - 7b_2^2b_4^3b_5^3 + 7b_1b_2^2b_4^3b_5^2 + 7b_1b_2^4b_4b_5^2 \\ &+ (4b_1^2b_2b_4b_7^2 + 4b_2b_4b_6^2b_7^2 - 8b_1b_2b_4b_5b_7^2 - 4b_2b_4^3b_7^2)c_1], \\ &- 7b_1b_2^2b_4^2b_5^4 - 7b_1b_2^4b_5^2b_6^2 - 7b_1b_2^2b_4^2b_5^2b_6^2 + 7b_1^2b_2^2b_4^2b_5^3 + 7b_2^2b_4^2b_5^3b_6^2 \\ &- 12b_1^2b_4b_6^3b_7^3 - 9b_1b_4^2b_6^4b_7^2 + 7b_1^2b_2^2b_4^2b_5b_6^2 + 12b_2^2b_4b_6^3b_7^3 - 7b_1^3b_2^2b_4^2b_6^2 \\ &+ 9b_1^2b_2^2b_5b_6^2b_7^2 - 12b_1b_2^2b_4b_5b_6b_7^3 + 4b_1b_2^2b_4^4b_7^2 + 7b_1^4b_2^2b_4^2b_5 - 4b_1^4b_4^2b_5b_7^2 \\ &+ 4b_1^2b_2^2b_4^2b_5b_7^2 - 9b_1b_2^2b_6^4b_7^2 + 7b_1^2b_4^4b_5b_6^2 + 4b_1^3b_4^2b_6^2b_7^2 - 4b_1b_2^2b_4^2b_6^2b_7^2 \\ &+ 4b_1^3b_4^2b_5^2b_7^2 - 9b_1b_2^2b_5^2b_6^2b_7^2 - 12b_1^2b_4b_5^2b_6b_7^3 - 9b_1b_4^2b_5^2b_6^2b_7^2 \\ &+ 12b_1^3b_4b_5b_6b_7^3 - 7b_1^3b_2^2b_4^2b_5^2 + 5b_1^2b_4^2b_5b_6^2b_7^2 + 9b_2^2b_5b_6^4b_7^2 + 12b_1b_4b_5b_6^3b_7^3 \\ &+ 9b_4^2b_5b_6^4b_7^2 - 7b_1^3b_4^4b_6^2 + 7b_1^4b_4^4b_5 - 7b_1^3b_4^4b_5^2 - 7b_1b_2^4b_5^4 \\ &+ 7b_2^4b_5^3b_6^2 + 7b_1^2b_2^4b_5^3 - 12b_2^2b_4^3b_6b_7^3 \\ &+ (4b_2^3b_6^2b_7^2 - 4b_1^2b_2b_5^2b_7^2 + 4b_1b_2b_5b_6^2b_7^2 + 4b_1^3b_2b_5b_7^2 \\ &-4b_1^2b_2b_6^2b_7^2 - 4b_1b_2^3b_5b_7^2 - 4b_2^3b_4^2b_7^2)c_1\Big) \end{aligned}$$

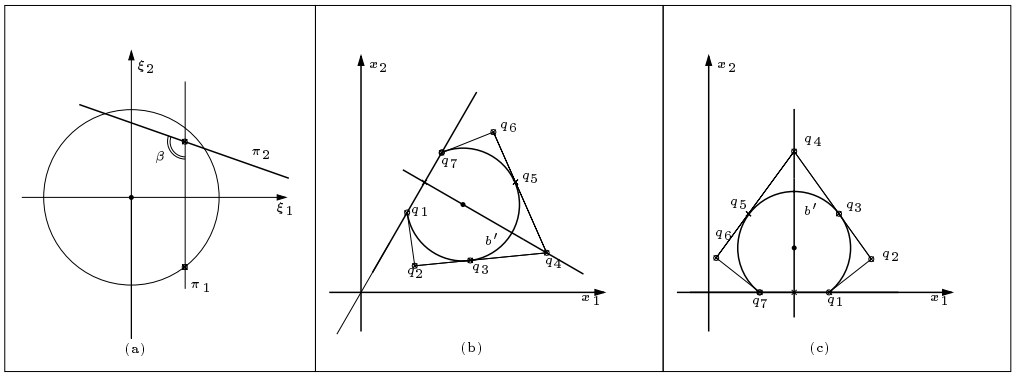

Fig. 13. (a) (ξ_1, ξ_2) section of the (ξ_1, ξ_2, ξ_3) space. The circle is a cross section of ball $B'(r)$ of radius $r_1 + r$. Line l, which is parallel to the ξ_3 axis, is the intersection of the planes π_1 and π_2, which in turn are the Voronoi planes separating $B'(r)$ and $B''(r)$ and separating $B'(r)$ and $B'''(r)$. (b) control points of the trimming curve that is part of the boundary of $b'(r)$ for Example 1. (c) the same control points for Example 2.

where

$$
\begin{aligned}
c_1 &= \sqrt{6b_1^2b_4^2 + 7b_2^2b_5^2 + 6b_1b_4b_6b_7} \\
d_1 &= b_7^2(b_1 + b_5)[(-b_1b_4b_5 - b_2^2b_4 - b_4b_6^2)c_1 \\
&\quad + b_1^2b_2b_4b_5 - b_1b_2b_4^3 + b_1b_2b_4b_6^2 - 3b_1b_2b_5b_6b_7 + 3b_2b_4^2b_6b_7 - 3b_2b_6^3b_7] \\
d_2 &= b_7^2(b_1 - b_5)[(b_1b_4b_5 - b_2^2b_4 - b_4b_6^2)c_1 \\
&\quad + b_1^2b_2b_4b_5 + b_1b_2b_4^3 - b_1b_2b_4b_6^2 - 3b_1b_2b_5b_6b_7 - 3b_2b_4^2b_6b_7 + 3b_2b_6^3b_7]
\end{aligned}
$$

We now need rational parametrizations of the circular arcs. The parametrization for arc $q_1 - q_2 - q_3$ is provided by

$$
(x_1, x_2) = \frac{(1-t)^2 q_3 + 2t(1-t)w_1 q_2 + t^2 q_1}{(1-t)^2 + 2t(1-t)w_1 + t^2} \quad , \quad 0 \le t \le 1 \; ,
$$

for a particular value for the weight w_1, which turns out to be the cosine of half the angle $\angle q_1 q_0 q_3$, or $\cos q_1 q_0 q_2$. This can be computed as

$$
w_1 = \frac{(q_1 - q_0) \cdot (q_2 - q_0)}{\|q_1 - q_0\| \|q_2 - q_0\|} \quad .
$$

Analogous parametrizations hold for arcs $q_3 - q_4 - q_5$ and $q_5 - q_6 - q_7$.

Here we place the balls in $\Re^3$ so that the line through the endpoints of a trimming arc is parallel to the x_1-axis in x_1x_2-space. Consider three balls B', B'', and B'''. Choose a coordinate system so that their centers are located at $(0,0,0)$, $(l_{12}\cos\alpha, -l_{12}\sin\alpha, 0)$, and $(l_{13}\cos(\beta-\alpha), l_{13}\sin(\beta-\alpha), 0)$ where l_{12} and l_{13} are the distances between the centers of B' and B'', and between the centers of B' and B''', respectively, β is the angle made by the three centers, with B' at the vertex $(0 < \beta < \pi)$, and

$$\alpha = \tan^{-1}\left[\frac{(a_3 + ra_4) - (a_1 + ra_2)\cos\beta}{(a_1 + ra_2)\sin\beta}\right] \quad .$$

With this definition we have that α is the angle between the ray through the centers of B' and B'', and the ξ_1-axis, and

$$\begin{aligned}\cos\alpha &= \frac{b_2\sin\beta}{(b_2^2 - 2b_2b_3\cos\beta + b_3^2)^{1/2}} \\ \sin\alpha &= \frac{b_3 - b_2\cos\beta}{(b_2^2 - 2b_2b_3\cos\beta + b_3^2)^{1/2}} \quad .\end{aligned}$$

Note that α is a function of r. This coordinate system is chosen so that the Voronoi planes defined below intersect at the ξ_1-axis.

Let the solvent ball have radius r. We consider the two planes π_1, π_2 relative to two trimming curves c_1, c_2. The position of the line $l = \pi_1 \cap \pi_2$ of intersection is used to track the intersection between c_1 and c_2 and to give their 2D NURBS representation.

With the above coordinate system, the two planes have equations:

$$\begin{aligned}\pi_1 &: (\cos\alpha)\xi_1 - (\sin\alpha)\xi_2 = a_1 + ra_2 \\ \pi_2 &: [\cos(\beta-\alpha)]\xi_1 + [\sin(\beta-\alpha)]\xi_2 = a_3 + ra_4\end{aligned}$$

where the a_i are the same as in Example 1:

$$a_1 = \frac{l_{12}^2 + r_1^2 - r_2^2}{2l_{12}} \qquad a_2 = \frac{r_1 - r_2}{l_{12}} \qquad a_3 = \frac{l_{13}^2 + r_1^2 - r_3^2}{2l_{13}} \qquad a_4 = \frac{r_1 - r_3}{l_{13}} \ ,$$

in accordance with (10).

The image of the trimming curve is the intersection of the spherical surfaces of the balls $B'(r)$ and $B''(r)$, which we define as the balls of radii $r_1 + r$ and

r_2+r centered at $(0,0,0)$ and $(l_{12}\cos\alpha, -l_{12}\sin\alpha, 0)$, respectively. The implicit equation of the spherical surface of $B'(r)$ is then $\xi_1^2+\xi_2^2+\xi_3^2=(r_1+r)^2$, and one finds that the ξ_3 coordinate of the two points of intersection between this sphere and the line l is

$$\xi_3 = \pm\sqrt{(r_1+r)^2-\xi_1^2-\xi_2^2}\ .$$

The segment of the line $l=\pi_1\cap\pi_2$ within $B'(r)$ then has the parametrization:

$$\begin{aligned}
&\xi_1 = (a_1+ra_2)/\cos\alpha \\
&\xi_2 = 0 \\
&\xi_3 = \sqrt{(r_1+r)^2-(a_1+ra_2)^2/\cos^2\alpha}\ u \quad , \\
&-1\le u\le 1 \quad .
\end{aligned}$$

To map the surface of the ball $B'(r)$ to a plane, we use an inverse mapping similar to (3) but for a sphere of radius r_1+r instead of 1 and specifically $d=2$:

$$\begin{aligned}
x_1 &= \frac{\xi_1}{r_1+r-\xi_3} \\
x_2 &= \frac{\xi_2}{r_1+r-\xi_3} \quad .
\end{aligned}$$

From this one obtains the intersection points q_1 and q_7 (see Figure 13(c)) in the $(x_1(r), x_2(r))$ parameter space as

$$\begin{aligned}
q_1 &= \left(\frac{b_1\cos\alpha-\sqrt{b_1^2\cos^2\alpha-b_2^2}}{b_2}, 0\right) \quad , \\
q_7 &= \left(\frac{b_1\cos\alpha+\sqrt{b_1^2\cos^2\alpha-b_2^2}}{b_2}, 0\right) \quad ,
\end{aligned}$$

and the trimming curve is an arc of the circle with center

$$q_0 = \left(\frac{b_1\cos\alpha}{b_2}, -\frac{b_1\sin\alpha}{b_2}\right)$$

and radius

$$\frac{b_6}{b_2} \quad .$$

In the x_1x_2-plane, line $\overleftrightarrow{q_1q_7}$ is just the x_1-axis, and line $\overleftrightarrow{q_8q_9}$ is $x_1 = b_1\cos\alpha/b_2$. We also have

$$q_8 = \left(\frac{b_1\cos\alpha}{b_2}, 0\right) , \qquad q_9 = \left(\frac{b_1\cos\alpha}{b_2}, -\frac{b_1\sin\alpha + b_6}{b_2}\right) .$$

From this we find that the break points q_3 and q_5 are

$$q_3 = \left(\frac{b_1\cos\alpha}{b_2} - \frac{(7b_6^2 - b_1^2\sin^2\alpha + 6b_1b_6\sin\alpha)^{1/2}}{4b_2}, -\frac{3}{4}\frac{b_1\sin\alpha + b_6}{b_2}\right)$$
$$q_5 = \left(\frac{b_1\cos\alpha}{b_2} + \frac{(7b_6^2 - b_1^2\sin^2\alpha + 6b_1b_6\sin\alpha)^{1/2}}{4b_2}, -\frac{3}{4}\frac{b_1\sin\alpha + b_6}{b_2}\right) .$$

We now determine q_2, q_4, and q_6 as the points of intersection of the tangent lines through q_1, q_3, q_5, and q_7. We get

$$q_4 = \left(\frac{b_1\cos\alpha}{b_2}, -\frac{b_1\sin\alpha}{b_2} + \frac{4b_6^2}{b_2(b_1\sin\alpha - 3b_6)}\right) .$$

Also

$$q_2 = \left(\frac{b_1\cos\alpha}{b_2} - \frac{3b_6^2(b_1\sin\alpha + b_6)}{b_2[b_1(c_2 - c_1)\sin\alpha + 3b_6c_1]} , \right.$$
$$\left. -\frac{b_1\sin\alpha}{b_2} + \frac{b_6^2(c_2 - 4c_1)}{b_2[b_1(c_2 - c_1)\sin\alpha + 3b_6c_1]}\right)$$

and

$$q_6 = \left(\frac{b_1\cos\alpha}{b_2} + \frac{3b_6^2(b_1\sin\alpha + b_6)}{b_2[b_1(c_2 - c_1)\sin\alpha + 3b_6c_1]} , \right.$$
$$\left. -\frac{b_1\sin\alpha}{b_2} + \frac{b_6^2(c_2 - 4c_1)}{b_2[b_1(c_2 - c_1)\sin\alpha + 3b_6c_1]}\right)$$

where

$$c_1 = \sqrt{b_1^2\cos^2\alpha - b_2^2} , \qquad c_2 = \sqrt{7b_6^2 - b_1^2\sin^2\alpha + 6b_1b_6\sin\alpha} .$$

6 Conclusions

We have described modeling and animation algorithms that dynamically update and render exact and smoothed molecular surface representations for growing collections of balls. Two main classes were considered: one where the radii of the atoms grow quadratically so that the Power Diagram remains fixed, and the other in which the atom radii grow linearly and the Power Diagram is updated continuously. In the first case accuracy of the solution is sacrificed for speed of the computation to allow fast user interaction times. In the latter case the exact solution is given at a higher computation cost for the case where higher accuracy is needed. The use of these algorithms can enable one to manipulate molecular models and smoothed molecular surfaces in a wide variety of applications.

Appendix A: Proof of equation (6)

Let the three circles be $(x - x_i)^2 + (y - y_i)^2 = r_i^2$, $i = 1, 2, 3$. Then the three corresponding planes are $(1 + x_i^2 + y_i^2 - r_i^2) - 2x_i\xi_1 - 2y_i\xi_2 + (1 - x_i^2 - y_i^2 + r_i^2)\xi_3 = 0$. Their point of intersection, if unique and finite, is given by $(\xi_1, \xi_2, \xi_3) = (D_1/D_4, D_2/D_4, D_3/D_4)$, where

$$D_1 = \begin{vmatrix} -1 - x_1^2 - y_1^2 + r_1^2 & -2y_1 & 1 - x_1^2 - y_1^2 + r_1^2 \\ -1 - x_2^2 - y_2^2 + r_2^2 & -2y_2 & 1 - x_2^2 - y_2^2 + r_2^2 \\ -1 - x_3^2 - y_3^2 + r_3^2 & -2y_3 & 1 - x_3^2 - y_3^2 + r_3^2 \end{vmatrix},$$

$$D_2 = \begin{vmatrix} -2x_1 & -1 - x_1^2 - y_1^2 + r_1^2 & 1 - x_1^2 - y_1^2 + r_1^2 \\ -2x_2 & -1 - x_2^2 - y_2^2 + r_2^2 & 1 - x_2^2 - y_2^2 + r_2^2 \\ -2x_3 & -1 - x_3^2 - y_3^2 + r_3^2 & 1 - x_3^2 - y_3^2 + r_3^2 \end{vmatrix},$$

$$D_3 = \begin{vmatrix} -2x_1 & -2y_1 & -1 - x_1^2 - y_1^2 + r_1^2 \\ -2x_2 & -2y_2 & -1 - x_2^2 - y_2^2 + r_2^2 \\ -2x_3 & -2y_3 & -1 - x_3^2 - y_3^2 + r_3^2 \end{vmatrix},$$

$$D_4 = \begin{vmatrix} -2x_1 & -2y_1 & 1 - x_1^2 - y_1^2 + r_1^2 \\ -2x_2 & -2y_2 & 1 - x_2^2 - y_2^2 + r_2^2 \\ -2x_3 & -2y_3 & 1 - x_3^2 - y_3^2 + r_3^2 \end{vmatrix}.$$

The condition that this point of intersection lies in the interior of B is

$$D_1^2 + D_2^2 + D_3^2 - D_4^2 < 0 \quad . \tag{11}$$

If $D_4 = 0$, then the point of intersection is at infinity, and the inequality (11) cannot be satisfied. (If $D_1 = D_2 = D_3 = D_4 = 0$, then the three planes have a line in common which intersects B, and it can be shown that the centers of the three circles are collinear and the circles intersect in two points.)

The intersection of three disks is bounded by three circular arcs exactly when each disk contains exactly one of the two points of intersection of the other two circles. In order for the first two circles to intersect in two points, we need that the distance between their centers is strictly between $|r_1 - r + 2|$ and $r_1 + r_2$. This can be expressed algebraically as

$$\begin{aligned} A_1 = &[(x_1 - x_2)^2 + (y_1 - y_2)^2 - (r_1 - r_2)^2] \\ &\cdot[(x_1 - x_2)^2 + (y_1 - y_2)^2 - (r_1 + r_2)^2] < 0 \quad . \end{aligned}$$

Next, we need that r_3 is between the distance from (x_3, y_3) to the two points of intersection of the first two circles. This condition turns out to be expressible as

$$\frac{\begin{vmatrix} x_1 & x_2 & x_3 \\ y_1 & y_2 & y_3 \\ 1 & 1 & 1 \end{vmatrix}^2 A_1 + A_2^2}{[(x_1 - x_2)^2 + (y_1 - y_2)^2]^2} < 0 \tag{12}$$

where

$$\begin{aligned} A_2 = &[(x_2 - x_1)(x_2 - x_3) + (y_2 - y_1)(y_2 - y_3)]r_1^2 \\ &+ [(x_2 - x_1)(x_3 - x_1) + (y_2 - y_1)(y_3 - y_1)]r_2^2 \\ &+ [(x_2 - x_1)^2 + (y_2 - y_1)^2] \\ &\cdot[(x_3 - x_1)(x_3 - x_2) + (y_3 - y_1)(y_3 - y_2) - r_3^2] \quad . \end{aligned}$$

Remarkably,

$$D_1^2 + D_2^2 + D_3^2 - D_4^2 = \begin{vmatrix} x_1 & x_2 & x_3 \\ y_1 & y_2 & y_3 \\ 1 & 1 & 1 \end{vmatrix}^2 A_1 + A_2^2 \quad .$$

Therefore, if the intersection of the three disks is bounded by three circular arcs ((12) and (12) hold), then the intersection point of the three planes is within B ((11) holds). If the intersection point of the three planes is a point within B ((11) holds), then (12) holds. Since (12) holds, we must have $A_1 < 0$, so that (12) holds as well, and then the three circles intersect pairwise in two points, and each disk contains exactly one of the two points of intersection of the other two circles.

References

[1] N. Akkiraju and H. Edelsbrunner. Triangulating the surface of a molecule. *Discrete Applied Mathematics*, 71:5–22, 1996.

[2] G. Albers and T. Roos. Voronoi diagrams of moving points in higher dimensional spaces. In *Proc. 3rd Scand. Workshop Algorithm Theory*, volume 621 of *Lecture Notes in Computer Science*, pages 399–409. Springer-Verlag, 1992.

[3] F. Aurenhammer. Power diagrams: Properties, algorithms, and applications. *SIAM Journal of Computing*, 16(1):78–96, 1987.

[4] C. L. Bajaj and W. J. Bouma. Dynamic Voronoi diagrams and Delaunay triangulations. In *Proc. 2nd Canadian Conference on Computational Geometry*, pages 273–277, 1990.

[5] C. L. Bajaj, H. Y. Lee, R. Merkert, and V. Pascucci. NURBS based B-rep models for macromolecules and their properties. In *Proceedings of the 4th Symposium on Solid Modeling and Applications*, pages 217–228, New York, May 1997. ACM Press.

[6] C. L. Bajaj and V. Pascucci. Splitting a complex of convex polytopes in any dimension. In *Proceedings of the Twelfth Annual Symposium On Computational Geometry (ISG '96)*, pages 88–97, New York, May 1996. ACM Press.

[7] C. L. Bajaj and V. Pascucci. Wrapping the Voronoi diagram: A constructive approach to duality. Technical report, University of Texas at Austin, 1997.

[8] C. L. Bajaj, V. Pascucci, A. Shamir, R. J. Holt, and A. N. Netravali. Multiresolution molecular shapes. Technical Report 99-42, TICAM, University of Texas at Austin, 1999.

[9] James F. Blinn. A generalization of algebraic surface drawing. *ACM Transactions on Graphics*, 1(3):235–256, July 1982.

[10] T. M. Y. Chan, J. Snoeyink, and C.-K. Yap. Output-sensitive construction of polytopes in four dimensions and clipped Voronoi diagrams in three. In *Proceedings of the Sixth Annual ACM-SIAM Symposium on Discrete Algorithms*, pages 282–291, San Francisco, California, January 1995.

[11] B. Chazelle. An optimal convex hull algorithm in any fixed dimension. *Discrete & Computational Geometry*, 10:377–409, 1993.

[12] L. P. Chew. Near-quadratic bounds for the L_1 Voronoi diagram of moving points. *Computational Geometry-Theory and Applications*, 7:73–80, 1997.

[13] M. L. Connolly. Analytical molecular surface calculation. *Journal of Applied Crystallography*, 16:548–558, 1983.

[14] M. L. Connolly. Solvent-accessible surfaces of proteins and nucleic acids. *Science*, 221:709–713, 1983.

[15] M. L. Connolly, T.J. O'Donnell, and S. Warde. Special issue on molecular surfaces. *Network Science*, 2(4), April 1996. M. L. Connolly "Molecular Surfaces: A Review", T.J. O'Donnell "The Scientific and Artistic Uses of Molecular Surfaces", S. Warde "Molecular Modeling and Simulation of Surfaces," http://edisto.awod.com/netsci/Issues/1996/Apr/articles.html.

[16] C. J. A. Delfinado and H. Edelsbrunner. An incremental algorithm for Betti numbers of simplicial complexes on the 3-sphere. *Computer Aided Geometric Design*, 12(7):771–784, 1995.

[17] Mathieu Desbrun and Marie-Paule Gascuel. Animating soft substances with implicit surfaces. In Robert Cook, editor, *SIGGRAPH 95 Conference Proceedings*, Annual Conference Series, pages 287–290, Los Angeles, August 1995. Addison Wesley.

[18] H. Edelsbrunner. *Algorithms in Combinatorial Geometry*, volume 10 of *EATCS Monographs on Theoretical Computer Science*. Springer-Verlag, Heidelberg, West Germany, 1987.

[19] H. Edelsbrunner. Smooth surfaces for multi-scale shape representation. In *Proc. 15th Conf. Found. Softw. Tech. Theoret. Comput. Sci.*, volume 1026 of *Lecture Notes in Computer Science*, pages 391–412. Springer-Verlag, 1995.

[20] H. Edelsbrunner. The union of balls and its dual shape. *Discrete & Computational Geometry*, 13(3-4):415–440, 1995.

[21] H. Edelsbrunner. Deformable smooth surface design. *Discrete & Computational Geometry*, 21:87–115, 1999.

[22] H. Edelsbrunner, M. Facello, and J. Liang. On the definition and the construction of pockets in macromolecules. Report UIUCDCS-R-95-1935, University of Illinois Urbana-Champaign, 1995.

[23] H. Edelsbrunner, D. G. Kirkpatrick, and R. Seidel. On the shape of a set of points in the plane. *IEEE Transactions on Information Theory*, IT-29:551–559, 1983.

[24] H. Edelsbrunner and E. P. Mücke. Three-dimensional alpha shapes. *ACM Transactions on Graphics*, 13(1):43–72, January 1994.

[25] H. Edelsbrunner and N. R. Shah. Incremental topological flipping works for regular triangulations. *Algorithmica*, 15:223–241, 1996.

[26] M. A. Facello. *Geometric Techniques for Molecular Shape Analysis*. PhD thesis, University of Illinois, 1996. Department of Computer Science Technical Report # 1967.

[27] J. J. Fu and R. C. T. Lee. Voronoi diagrams of moving points in the plane. *International Journal of Computational Geometry and Applications*, 1(1):23–32, 1991.

[28] T. Fujita, K. Hirota, and K. Murakami. Representation of splashing water using metaball model. *Fujitsu*, 41(2):159–165, 1990. in Japanese.

[29] G. Graves. The magic of metaballs. *Computer Graphics World*, 16(5):27–32, 1993.

[30] L. Guibas, J. S. B. Mitchell, and T. Roos. Voronoi diagrams of moving points in the plane. In *Proc. 17th Internat. Workshop Graph-Theoret. Concepts Comput. Sci.*, volume 570 of *Lecture Notes in Computer Science*, pages 113–125. Springer-Verlag, 1991.

[31] P. M. Hubbard. Approximating polyhedra with spheres for time-critical collision detection. *ACM Transactions on Graphics*, 15(3), 1996.

[32] H. Imai, M. Iri, and K. Murota. Voronoi diagram in the Laguerre geometry and its applications. *SIAM Journal of Computing*, 14:93–10, 1985.

[33] S. Krishnan, D. Manocha, and A. Narkhede. Representation and evaluation of boolean combinations of NURBS solids. In *Fifth MSI-Stony Brook Workshop on Computational Geometry, Stony Brook*, October 1995.

[34] S. Kumar, D. Manocha, and A. Lastra. Interactive display of large-scale NURBS models. *IEEE Transactions on Visualization and Computer Graphics*, 2(4):323–336, 1996.

[35] B. Lee and F. M. Richards. The interpretation of protein structures: Estimation of static accessibility. *Journal of Applied Crystallography*, 55:379–400, 1971.

[36] N. L. Max. Computer representation of molecular surfaces. *IEEE Computer Graphics and Applications*, 3(5):21–29, August 1983.

[37] H. Nishimura, M. Hirai, T. Kawai, T. Kawata, I. Shirakawa, and K. Omura. Object modeling by distribution function and a method of image generation. *Transactions IECE Japan, Part D*, J68-D(4):718–725, 1985.

[38] T. Nishita and E. Nakamae. A method for displaying metaballs by using Bézier clipping. In *Computer Graphics Forum*, volume 13, pages 271–280. Eurographics, Basil Blackwell Ltd, 1994. Eurographics '94 Conference issue.

[39] T. Roos. Voronoĭ diagrams over dynamic scenes. *Discrete Applied Mathematics. Combinatorial Algorithms, Optimization and Computer Science*, 43(3):243–259, 1993.

[40] T. Roos. New upper bounds on Voronoi diagrams of moving points. *Nordic Journal of Computing*, 4(2):167–171, 1997.

[41] M. F. Sanner and A. J. Olson. Reduced surface: An efficient way to compute molecule surfaces. *Biopolymers*, 38:305–320, 1996.

[42] M. F. Sanner and A. J. Olson. Real time surface reconstruction for moving molecular fragments. In *Proceedings of the Pacific Symposium on Biocomputing '97*, Maui, Hawaii, January 1997.

[43] M. F. Sanner, A. J. Olson, and J. C. Spehner. Fast and robust computation of molecular surfaces. In *Proc. 11th Annual ACM Symposium on Computational Geometry*, pages C6–C7, 1995.

[44] D. Terzopoulos and H. Qin. Dynamic NURBS with geometric constraints for interactive sculpting. *ACM Transactions on Graphics*, 13(2):103–136, 1994.

[45] A. Varshney and F. P. Brooks, Jr. Fast analytical computation of Richard's smooth molecular surface. In Gregory M. Nielson and Dan Bergeron, editors, *Proceedings of the Visualization '93 Conference*, pages 300–307, San Jose, CA, October 1993. IEEE Computer Society Press.

[46] R. Voorintholt, M. T. Kosters, and G. Vegter. A very fast program for visualizing protein surfaces, channels and cavities. *Journal on Molecular Graphics*, 7:243–245, December 1989.

[47] J. Wernecke. *The Inventor Mentor.* Addison–Wesley, 1994.

[48] J. Bloomenthal with C. Bajaj, J. Blinn, M.-P. Cani-Gascuel, A. Rockwood, B. Wyvill, and G. Wyvill, editors. *Introduction to Implicit Surfaces.* Morgan Kaufmann Publishers, San Francisco, 1997.

[49] B. Wyvill, C. McPheeters, and G. Wyvill. Animating soft objects. *The Visual Computer*, 2(4):235–242, 1986.

[50] B. Wyvill, C. McPheeters, and G. Wyvill. Data structure for soft objects. *The Visual Computer*, 2(4):227–234, 1986.

[51] S. Yoshimoto. Ballerinas generated by a personal computer. *Journal of Visualization and Computer Animation*, 3(2):55–90, 1992.